A LABORATORY MODEL OF PLANETARY AND STELLAR CONVECTION

J. E. Hart, J. Toomre, A. E. Deane, and N. E. Hurlburt
Department of Astrophysical, Planetary and Atmospheric Sciences
and Joint Institute for Laboratory Astrophysics
University of Colorado, Boulder, Colorado 80309

G. A. Glatzmaier
Los Alamos National Laboratory, Los Alamos, New Mexico 87545

G. H. Fichtl, F. Leslie, and W. W. Fowlis
NASA Marshall Space Flight Center, Huntsville, Alabama 35812

P. A. Gilman
High Altitude Observatory
National Center for Atmospheric Research, Boulder, Colorado 80307

ABSTRACT

Experiments on thermal convection in a rotating, differentially-heated spherical shell with a radial buoyancy force were conducted in an orbiting microgravity laboratory. A variety of convective structures, or planforms, were observed, depending on the magnitude of the rotation and the nature of the imposed heating distribution. The results are in agreement with numerical simulations that can be conducted at modest parameter values, and suggest possible regimes of motion in rotating planets and stars.

DISCUSSION

Large-scale atmospheric motions on rotating planets and stars are influenced by both buoyancy and Coriolis forces. On a spherical surface the Coriolis force varies with latitude, and this variation is thought to be a fundamental influence in a wide range of phenomena of interest to geophysicists and astrophysicists. These phenomena include cloud-band orientation in planetary atmospheres, differential rotation in the solar atmosphere, the formation of jet-streams, and magnetic dynamo action. Except for flows that are homogeneous, so that buoyancy-driven motions are absent, it has been impossible to properly model even the simplest global motions in the terrestrial laboratory. When the rotation vector Ω is inclined to Earth's gravity g an oscillatory body force results that has no geophysical analog. Therefore, previous laboratory experiments on global circulations have been confined either to: (a) studies of convection near the poles where Ω and g are nearly parallel and the geometry is effectively flat [1], or to (b) studies of motions close to the equator where Ω and g are nearly perpendicular, with the effects of gravity being simulated by centrifugal buoyancy forces associated with very rapid rotation [2,3]. Our laboratory model, which consistently simulates global convective motions in a spherical shell of incompressible fluid, is based on the existence of density-dependent electrostatic forces in a dielectric medium. Because these forces are relatively weak, it is necessary to operate the experiment in an environment where g is small. This report describes our instrument, the "Geophysical Fluid Flow Cell," and outlines results from experiments carried out during its flight aboard the Spacelab 3 microgravity laboratory.

The motion of an incompressible fluid is entirely governed by the vorticity equation, obtained by taking the curl of the momentum equations. In a dielectric liquid subject to imposed electric field gradients, there will be polarization forces present in addition to normal buoyancy. The non-conservative part of these forces contribute to vorticity generation. As shown in Reference 4 this generation is proportional to

$$\text{curl (body force)} = \alpha \, \nabla T \times \nabla \Phi + \frac{\epsilon \gamma}{2} \nabla T \times \nabla E^2 \quad , \tag{1}$$

where α is the thermal expansivity, T is the temperature, Φ is the geopotential, E is the electric field, ϵ is the average dielectric constant of the liquid, and γ is the relative change of dielectric constant with temperature. In a self-gravitating fluid Φ is an inverse function of radius r. We would like the first and second terms on the right hand side of equation (1) to be isomorphic functions. A simulation of thermal buoyancy in a radial geopotential may be attained when an electric field $E \cong r^{-2} \, r$ is generated in the liquid by applying a uniform electric potential across two concentric spherical surfaces. The resulting electrostatic "gravity," which is proportional to ∇E^2, varies like r^{-5} instead of r^{-2}, as might be desired, but it has been shown theoretically that the unstable eigenfunctions and other properties of thermal convection in a non-rotating spherical shell containing a Boussinesq liquid are essentially unaffected by this difference [5]. The magnitude of the electrostatic "gravity" is limited by the breakdown field strength of existing low-viscosity, low-loss dielectrics to about 0.1 g's (or 1 ms^{-2}) in an apparatus of reasonable size. Thus the use of electrodynamic forces to study convection in spherical shells is only practical in the microgravity environment of the Shuttle orbiter.

A diagram of the cell used in our experiment is shown in Figure 1. A dielectric silicone oil of 0.65 centistoke viscosity is contained between two hemispherical shells that form part of a spherical capacitor. We study fluid motions in a single hemisphere because non-radial electric fields occur in the vicinity of the inner sphere's mechanical support which spans the annular gap near the south pole. The inner shell at radius R_i is made of polished nickel, and the outer at radius R_o is a transparent sapphire dome about 1 cm thick. Temperatures are maintained along both these surfaces by a system of heater coils and thermistor sensors installed in a computer-controlled servo loop. The thermal boundary conditions are axisymmetric, but allow for variations of both inner (T_i) and outer (T_o) surface temperature with latitude θ. Although uniform differential heating, with $T_i > T_o$ and independent of θ, is the simplest and most relevant case for modelling objects with spherically symmetric forcing, several experiments were run with a hotter pole. Such statically unstable non-uniform heating is thought to occur in rapidly rotating stars, giving rise to a meridional circulation [6-8] with little-known non-axisymmetric instability properties. Theoretical studies have shown that the spatial patterns or planforms selected by global convective modes are strongly influenced by latitudinal gradients, and that this selection may possibly be related to the structure of Jovian cloudbands [9,10]. To generate the electrostatic gravity, a 300 Hz alternating potential V_o is applied to a transparent conducting coating on the inner wall of the outer hemisphere. The inner sphere is grounded. The field reverses in a period short compared to the charge relaxation time for the fluid. This ensures an absence of electric currents and associated non-geophysical instabilities. In addition the oil has such a low dielectric loss that internal dissipative heating, even with potentials as high as 10 kV, is entirely negligible. The cell assembly including the high-voltage supply and the thermal-control circuitry is mounted on a rotating turntable that maintains a constant but adjustable rotation rate Ω.

Flows are visualized by Schlieren and shadowgraph photography. A non-rotating optical train focuses light from a grating onto the inner sphere. Thermally induced refractive index variations in the fluid cause individual rays to bend. When the incident rays are compared with the reflected rays, various

measures of the radially-averaged temperature field in the fluid are obtained. Because of space and weight limitations the optical system does not image the whole hemisphere; rather, a circular view extending from equator to pole and covering a quadrant in longitude reaching ±63 deg at 45 deg north is obtained (Fig. 2).

There are several non-dimensional numbers that serve to define the convective flow regimes. The fixed parameters are the Prandtl number P_r = (viscosity ν)/(thermal diffusivity κ) = 8.4 and the aspect ratio R_i/R_o = 2.402 cm/3.300 cm = 0.73. The measure of rotation is taken to be the Taylor number

$$T_a = \frac{4\Omega^2(R_o - R_i)^4}{\nu^2} \tag{2}$$

The Rayleigh number indicates the degree of thermal forcing with respect to dissipation. It is defined by

$$R_a = g_o \frac{\alpha\Delta T_r(R_o - R_i)^3}{\nu\kappa} \tag{3}$$

where g_o is the equivalent electrostatic gravity at $r = R_o$ and $\Delta T_r \equiv T_i - T_o$ is the radial temperature difference across the fluid at the equator. Finally, $H \equiv \Delta T_\theta/\Delta T_r$ compares the imposed pole-to-equator temperature difference at the boundaries to the radial temperature difference (with H vanishing for uniform heating).

A sequence of Schlieren images for cases with uniform imposed temperature on each hemisphere (H = 0) is shown in Figure 3. In Figure 3A the Taylor number is relatively small and rotational effects are weak. At a Rayleigh number above about 2×10^3, convective instabilities form and break the spherical symmetry of the conductive thermal balance that exists at smaller R_a. The tessellated pattern shows little influence of rotation, and evolves slowly with time. The patterns are suggestive of those predicted by a theory [11] for planform selection in a non-rotating shell without the rigid equatorial boundary. The observed convection has narrow updrafts along the edges of the cells and broad sinking regions in cell centers. One possible explanation is that this is a result of radial asymmetry in the "gravity" which is concentrated near the inner sphere. For example, it has been shown [12] that planar convection in a layer with unstable thermal gradients concentrated near the lower wall is dominated by hexagons with downflow in the center and upflow at the edges. Another explanation, suggested by similar results from our numerical simulations of flows with either r^{-2} or r^{-5} gravity, is that the narrow updrafts are a result of strong nonlinear interactions in the spherical geometry.

As the Taylor number is increased, the influence of rotation becomes larger (Fig. 3B). The weakly supercritical convective modes begin to feel the Taylor-Proudman constraint [13] that the motion should be invariant in the direction of Ω. In agreement with earlier analytical and numerical calculations [14,15] the boundaries of the convection cells are aligned in the north-south direction. The convection dies out somewhat north of the critical latitude on the outer boundary, here 43 deg, where a tangent cylinder drawn parallel to Ω just intersects the inner sphere at the equator. These low-latitude "banana cells" have a prograde propagation which is revealed in extended sequences of shadowgraph images. The banana cells dominate the weakly unstable flows (i.e., modest R_a) at all T_a greater than about 10^4. However, as R_a is increased, mid-latitude and polar modes become unstable as well. In Figure 3C, interactions with retrograde-propagating mid-latitude convection modes occur at the tips of the banana cells.

33

This causes a wavering and, at higher R_a, a nearly complete erosion of the banana cells. In Figure 3D, vestiges of the Taylor-Proudman constraint are found only within 20 deg of the equator. The remaining convection is highly turbulent, more horizontally isotropic, and contains most of the rms temperature variance.

A series of experiments with H = 1 is illustrated in Figure 4. Because the pole is hotter than the equator on each boundary, there is no purely conductive motionless state. A meridional circulation always exists, and with even a small amount of rotation substantial zonal flows will be generated. The interaction of this axisymmetric motion with incipient non-axisymmetric convective instabilities leads to the spiral pattern of convection at low T_a (Fig. 4A). The cells tip west (to the right) as one follows an updraft equatorward. The updrafts are narrow and the downdrafts are broad. If R_a is increased at this T_a (Fig. 4B), the thermal fronts along the spiral wave boundaries sharpen and a secondary instability occurs. The resulting defects lead to an irregular pattern that evolves chaotically in time. At larger T_a banana cells reappear at low latitudes. However, irregular spiral waves persist at high latitudes, becoming more axisymmetric (Fig. 4C). At high T_a and high R_a (Fig. 4D) a very complicated turbulent flow is observed. Imbedded in the circulation are fairly stable, mid-latitude, triangularly-shaped waves that appear to be coupled to the low-latitude banana cells. None of the experiments with H = 0 to 2, R_a = 10^3 to $\cong 10^5$, T_a = 10^3 to $\cong 10^6$ produced any axisymmetric tropical convection resembling, say, Jovian cloud band structure or orientation.

Numerical solution of the governing Boussinesq hydrodynamic equations is practical with super-computers for some of the lower R_a cases studied experimentally. We have solved the nonlinear three-dimensional problem in spherical geometry using a spectral transform method [16]. The velocity and thermodynamic functions are expanded in spherical harmonics in longitude and latitude, and Chebyshev polynomials in radius. All the conditions of the laboratory experiment are modelled except for the no-slip velocity constraint at the equatorial barrier, which is replaced by a stress-free condition. Computations using a slower finite-difference model, in which the proper equatorial condition can be implemented, indicate that it exerts only a minor quantitative effect on the solutions, although the equatorial barrier may affect the direction of the relatively weak phase propagation at modest T_a. Figure 5A shows the mid-depth radial velocity pattern, which is essentially the same as the radially-averaged thermal pattern, for the conditions of Figure 3B. Although there is some wavering of the banana cells, the mid-latitude modes are weak. The thermal spectrum peaks near wavenumber m = 15 (Fig. 6A); the pattern translates westward (retrograde) at a low rate of $\cong 0.45$ deg per rotation. The experiment is dominated by wavenumber 15, in good agreement with the calculation. The differential rotation produced in the numerical model is retrograde at the equator and contributes about 1 percent to the total kinetic energy. The experiment confirms previous predictions [17, 18] that both rigid boundary conditions and the relatively high Prandtl number tend to suppress differential rotation, when compared to the large zonally-averaged flows predicted in models of solar convection with stress-free boundaries and a Prandtl number of unity [19]. A numerical simulation of a rapidly rotating and more unstable case is shown in Figure 5B for the same conditions as Figure 3C. The calculated flow now includes a substantial contribution from polar and mid-latitude modes that are observed to interact with the tips of the banana cells exactly as seen in the experiment. The thermal spectrum (Fig. 6B) is broad with a wave maximum at longitudinal wavenumber 17 which compares favorably with the experimental value of 18. In this case the computed differential rotation is concentrated near the poles with a structure that depends on the meridional circulation there. Typically there is downward flow at the pole with prograde differential rotation in the upper part of the fluid shell and retrograde differential rotation in the lower part. Details of the maintenance of the differential rotation and other aspects of the computed solutions will be reported separately [20]. Further calculations aimed at understanding the spiral waves which occur at H $\simeq$ 1, and their interactions with the banana cells, are underway.

The experiments have supplied new data on pattern selection and low and mid-latitude inter-actions in rotating thermally unstable flows. Physical interpretation of these results, and future experiments planned on secondary instability and the transition to turbulence, should provide new insights into nonlinear processes important in the dynamics of planetary and stellar convection.

REFERENCES AND NOTES

1. Rossby, H. T.: J. Fluid Mech., Vol. 36, 1969, p. 309.

2. Busse, F. H. and Carrigan, C. R.: Science, Vol. 191, 1976, p. 81.

3. Carrigan, C. R. and Busse, F. H.: J. Fluid Mech., Vol. 126, 1983, p. 287.

4. Hart, J. E.: NASA Report CR-2753, 1976, 66 pp. A general discussion of electrohydrodynamics is provided by J. R. Melcher and G. I. Taylor [Annu. Rev. Fluid Mech., Vol. 1, 1969, p. 111]. An implementation of this concept in cylindrical geometry is presented by B. Chandra and D. E. Smylie [Geophys. Fluid Dyn., Vol, 3, 1972, p. 211].

5. Hart, J. E. and Toomre, J.: NASA Report NAS8-31958, 1977, 65 pp. For aspect ratios R_i/R_o smaller than that used in our instrument the differences can become significant.

6. Eddington, A. J.: Observatory, Vol. 48, 1925, p. 73.

7. Sweet, P. A.: Mon. Not. Roy. Astron. Soc., Vol. 110, 1950, p. 548.

8. Tassoul, J. L.: Theory of Rotating Stars, Princeton University Press, 1978.

9. Hathaway, D. H., Gilman, P. A., and Toomre, J.: Geophys. Astrophys. Fluid Dyn., Vol. 13, 1979, p. 287.

10. Hathaway, D. H., Toomre, J., and Gilman, P. A.: Geophys. Astrophys. Fluid Dyn., Vol. 15, 1980, p. 7.

11. Busse, F. H.: J. Fluid Mech., Vol. 72, 1975, p. 67.

12. Krishnamurti, R.: J. Atmos. Sci., Vol. 32, 1975, p. 1353.

13. Greenspan, H. P.: The Theory of Rotating Fluids, Cambridge Univ. Press, 1968.

14. Busse, F. H.: J. Fluid Mech., Vol. 44, 1970, p. 441.

15. Gilman, P. A.: J. Atmos. Sci., Vol. 32, 1975, p. 1331.

16. Glatzmaier, G. A.: J. Computational Phys., Vol. 55, 1984, p. 461.

17. Gilman, P. A.: Geophys. Astrophys. Fluid Dyn., Vol. 11, 1978, p. 181. For the same values of Rayleigh, Taylor, and Prandtl numbers, no-slip boundaries for convection in a spherical shell reduce the induced differential rotation kinetic energy by a factor of about 25, compared to the stress-free boundary case [see (19)].

18. Gilman, P. A.: J. Fluid Mech., Vol. 57, 1973, p. 381. Although this calculation is for a thin annulus in Cartesian geometry rather than a spherical shell, it shows that the induced differential rotation kinetic energy for a Prandtl number of 8 is reduced, relative to the convection kinetic energy that drives it, by about a factor of 8 when compared to the Prandtl number unity case (approximately a linear relationship in this Prandtl number range).

19. Gilman, P. A.: Geophys. Astrophys. Fluid Dyn., Vol. 8, 1977, p. 93.

20. Glatzmaier, G. A, Hart, J. E., and Toomre, J.: in preparation.
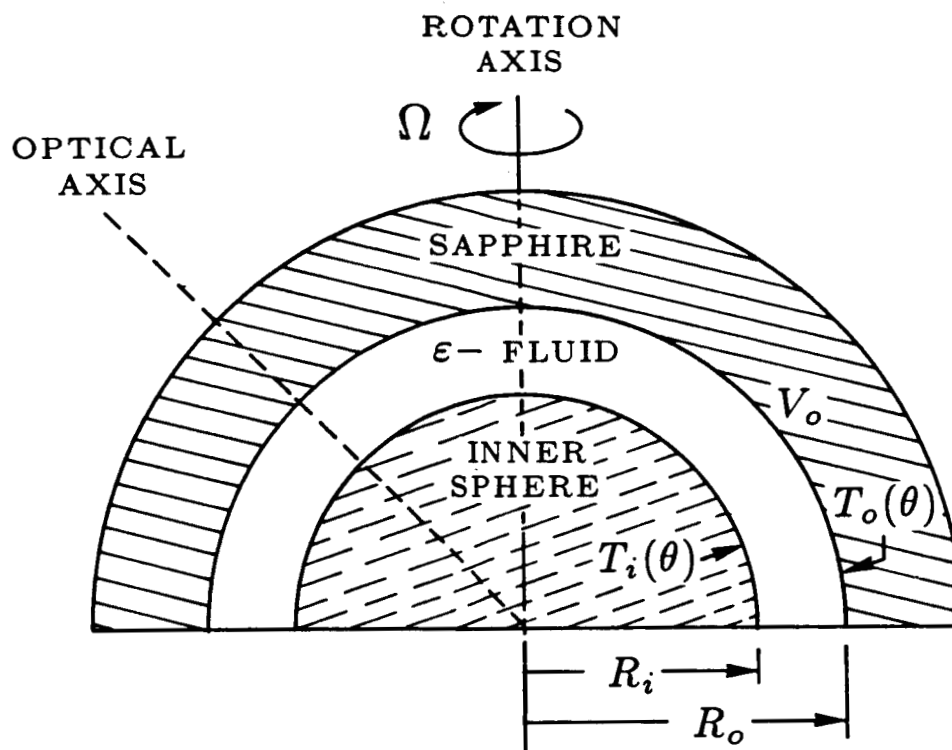
Figure 1. Cross-section of the experimental cell used to study thermal convection under the effects of rotation Ω in a hemispherical shell of fluid in the presence of an electrical analog of a radial gravity field. The inner radius of the shell of fluid is $R_i = 2.4$ cm and the outer radius $R_O = 3.3$ cm. The electrostatic gravity is achieved by imposing an alternating electrical potential V_O across the fluid shell. The dielectric silicone working fluid is bounded on the outside by a transparent sapphire dome to allow optical probing of the convective flows and thermal structures that result from differential heating.
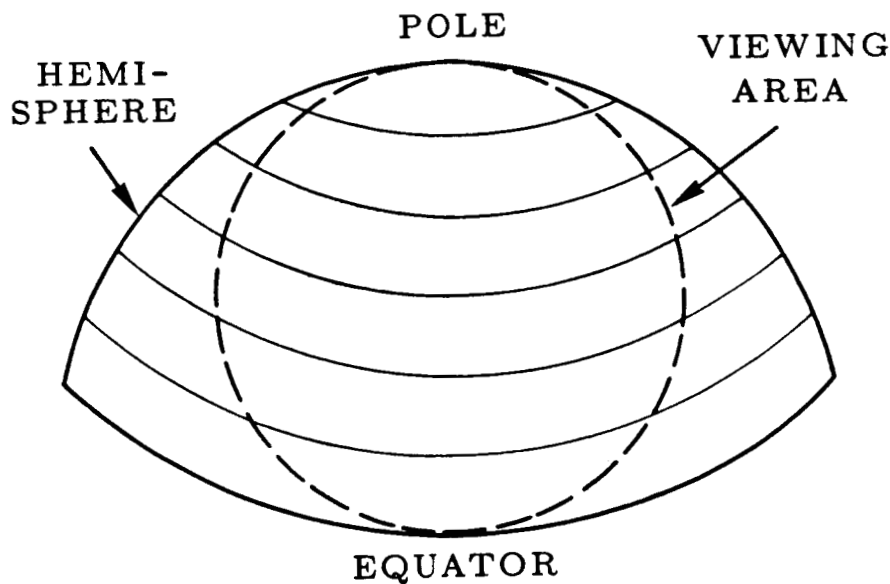
Figure 2. Sketch of the Schlieren viewing configuration with respect to the hemispherical shell.
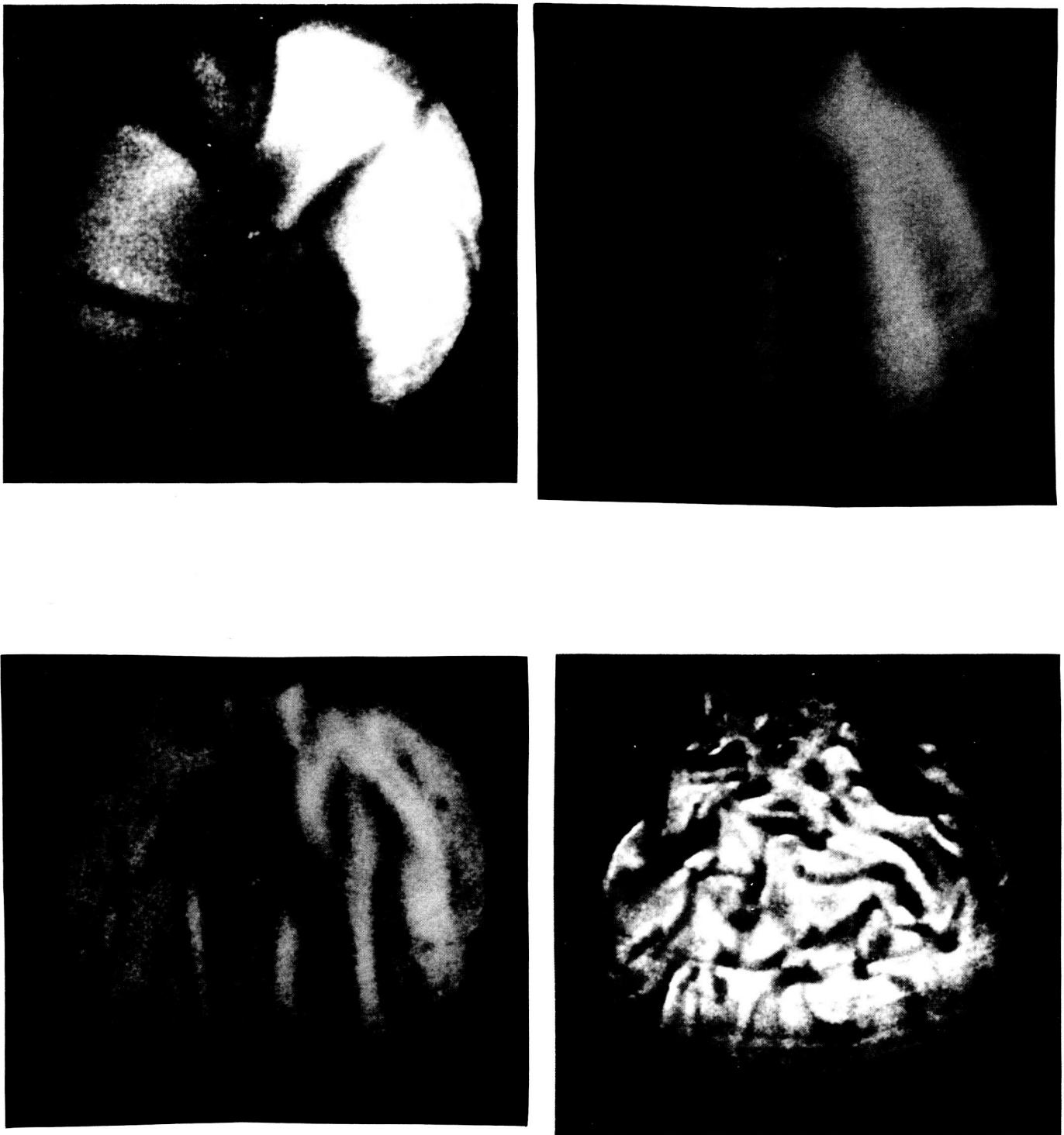
Figure 3. Planforms for the convection as observed with Schlieren photography in experiments with a uniform radial temperature difference imposed between the inner and outer spheres. (H = 0). These circular views of a portion of the hemisphere extend from the pole at the top to the equator at the bottom, as indicated in Figure 2. The basic rotation is from right (west) to left (east).
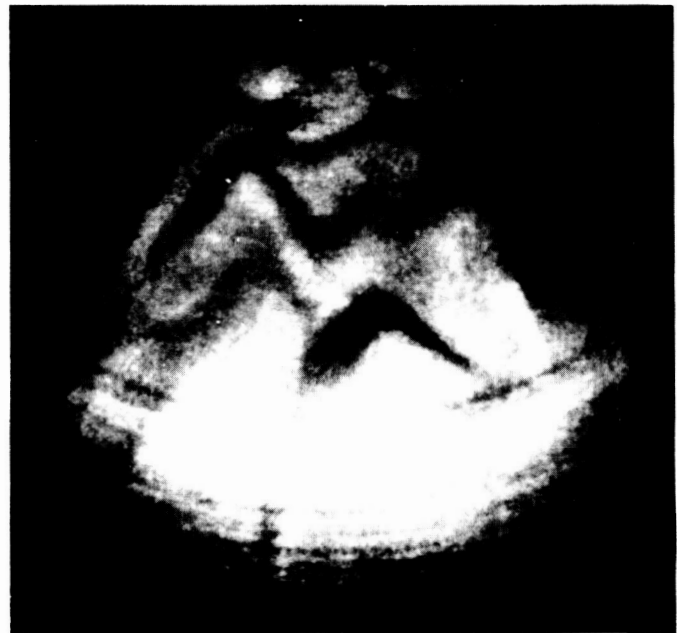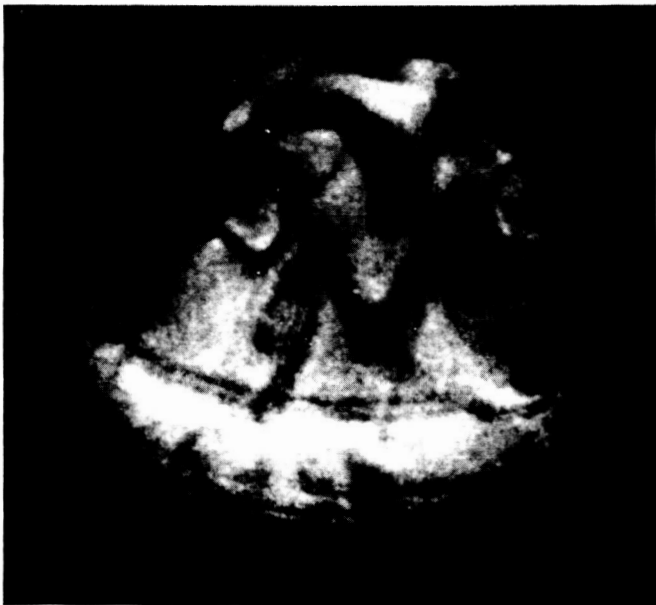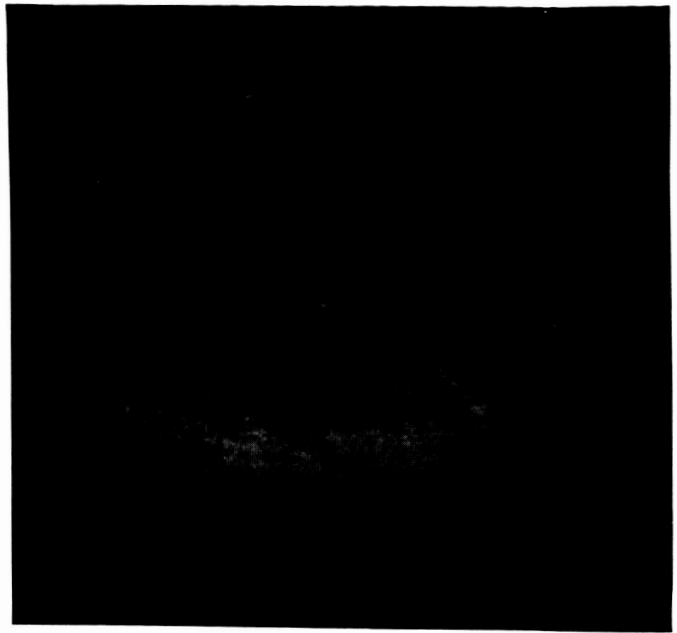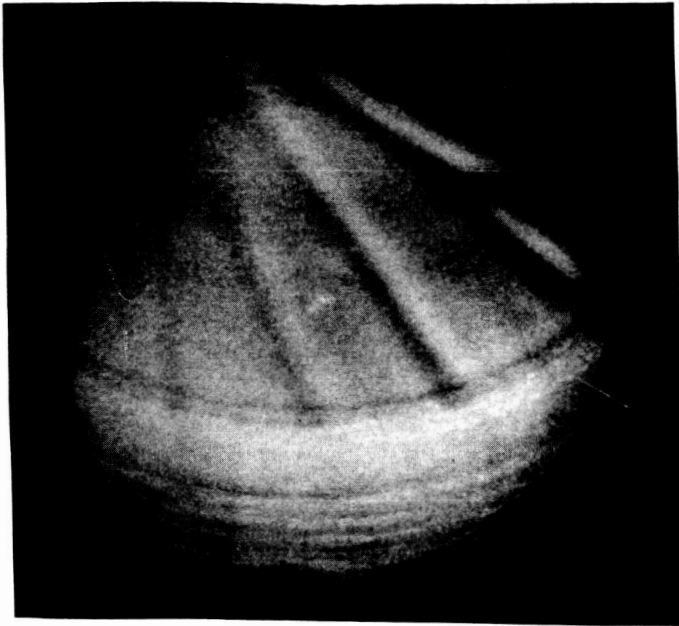
Figure 4. Planforms for the convection observed in experiments with temperature increasing
poleward on each spherical boundary in addition to a uniform radial temperature
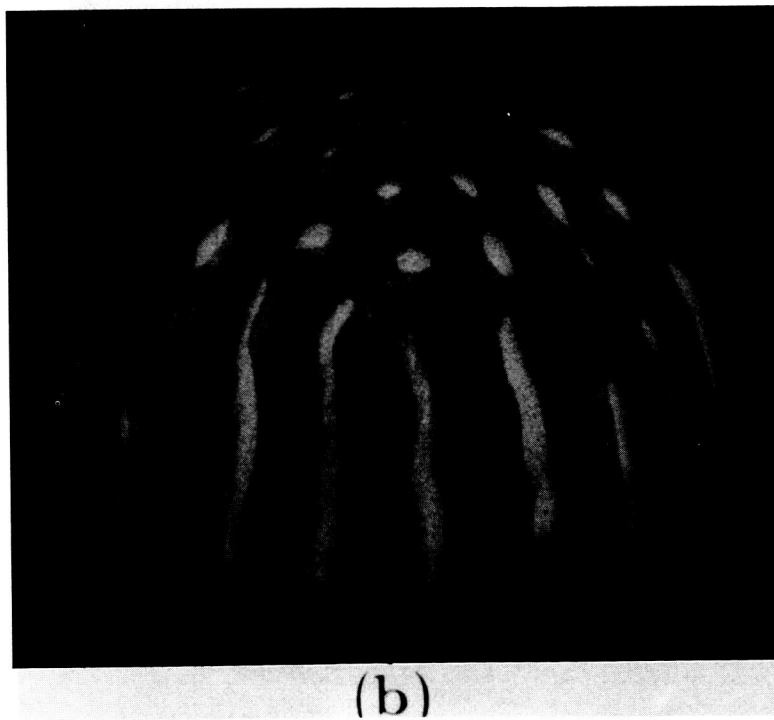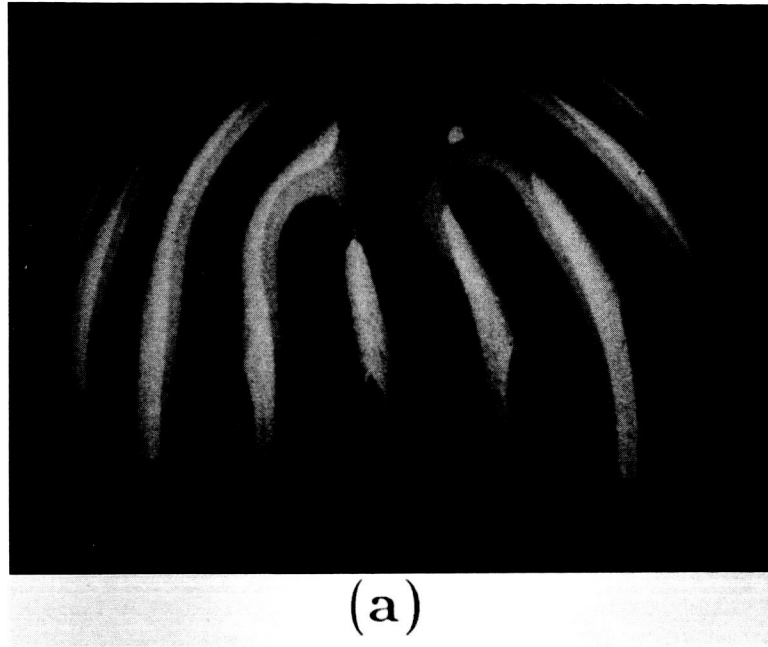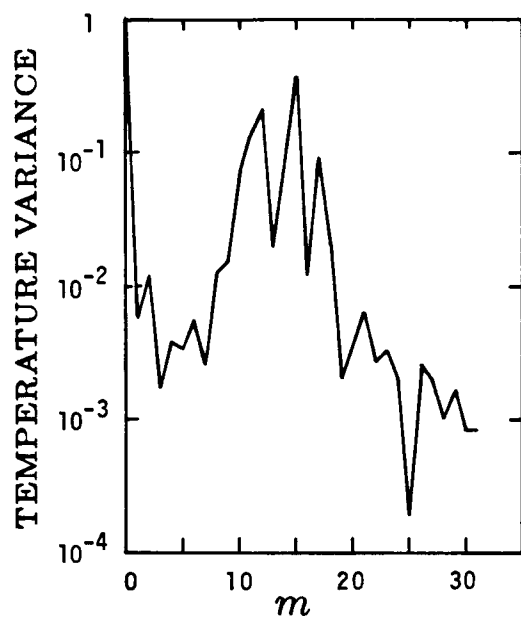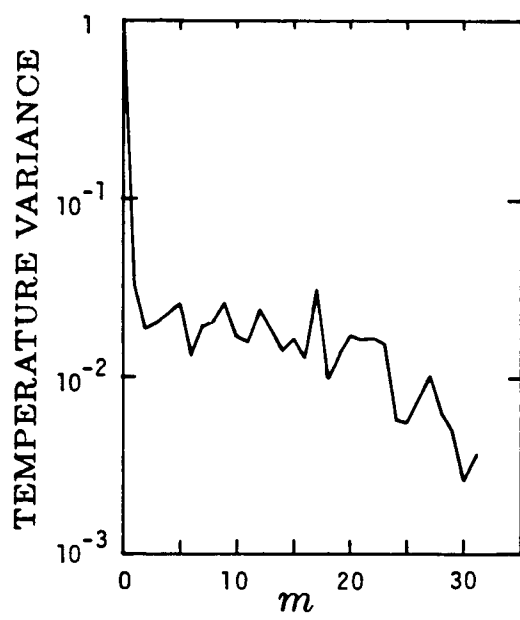difference between the spheres (H = 1).

(a)

(b)

Figure 5. Surface plots of computed radial velocity at mid-depth in a rotating hemispherical shell as obtained from three-dimensional numerical simulations. (A) For conditions corresponding to those in Figure 3B and (B) to those in Figure 3C.

Figure 6. Latitudinally and radially-averaged rms temperature variance as a function of longitudinal wavenumber m for the numerically computed flows of Figures 5A and 5B.